


Article

Cross-Axis Coupling Effects in Single-Axis Nuclear Magnetic Resonance Gyroscopes

Zhiguo Wang * , Yi Zhang, Xiang Zhan, Qiyuan Jiang and Hui Luo

College of Advanced Interdisciplinary Studies, and Interdisciplinary Center of Quantum Information, National University of Defense Technology, Changsha 410073, China; abnormal_zy@163.com (Y.Z.); zhanxiang09@163.com (X.Z.); qiyuanjiang1990@163.com (Q.J.); luohui.luo@163.com (H.L.)

* Correspondence: maxborn@nudt.edu.cn

Received: 11 December 2019; Accepted: 27 January 2020; Published: 29 January 2020



Abstract: Nuclear magnetic resonance gyroscopes (NMRGs) may be operated in an environment with violent vibration that usually contains both linear components and angular components. To analyze the influence of angular vibration on an NMRG, cross-axis coupling effects are studied. The cross-axis rotation rates induce an equivalent magnetic field. Its influence can be described by the Bloch equations. The approximate frequency shift and amplitude of the spin oscillator with an equivalent magnetic field in the cross-axis were obtained, which was validated by numerical simulation. The findings show that the angular vibration component leads to a remarkable error for the NMRG. When the angular vibration frequency is near the Larmor frequency, the oscillation frequency of the spins may be locked to the angular vibration frequency, destroying the NMRG's ability to measure rotation rates. The cross-axis coupling problem should be considered in the design of an NMRG and corresponding inertial navigation systems.

Keywords: nuclear magnetic resonance gyroscope; cross-axis coupling; magnetic field; rotation rate; frequency shift

1. Introduction

A nuclear magnetic resonance gyroscope (NMRG) measures rotation rates through the detection of the Larmor precession frequency of atomic spins in a static magnetic field [1–4]. Its physical foundation can be traced back to the pioneering work done by Larmor in 1895, Rabi in 1938, Bloch et al. in 1946 [5,6]. Leete filed a patent application on NMRG in 1952, which was assigned to the General Electric Company. Since then, several other companies conducted research on the NMRG. Both Singer and Litton had demonstrated NMRG prototypes with navigation grade in the 1980s [7]. However, compared with optical gyroscopes developed in the same period, the NMRG did not show enough advantages. Therefore, research on the NMRG entered a low tide.

The turnaround took place in the 2000s when micro-fabrication technology became more and more mature [7]. NMRGs have attracted considerable attention due to potential advantages including small size, weight and power. It is believed that the NMRG is an ideal sensor for inertial applications, since it has no mechanical part and is thus insensitive to mechanical shock and vibration [6–8]. The NMRG has already achieved near navigation-grade performance with a volume of 10 cm³ [5], indicating a bright prospect for mass applications.

The NMRG has the greatest sensitivity to the axis along the applied static field, but it can be affected by cross-axis rotation rates as well [9,10]. That is, the NMRG is not a true single-axis gyroscope. Physically, the NMRG is essentially a spin oscillator that is easily affected by a magnetic field, regardless of it being a true or equivalent magnetic field [9–12]. The magnetic field shield suppresses the external magnetic field but cannot suppress the equivalent magnetic field due to mechanical rotation.

The cross-axis coupling effects for a cryogenic ^3He gyroscope have been investigated in detail [9,10]. The relaxation time for ^3He can be as long as 140 h, which makes the relaxation in the dynamical equation of spins negligible, and the ^3He gyroscope can be operated in an open-loop mode [10]. It was clear that cross-axis rotation will degrade the performance of an NMRG. Recently, it was found that an NMRG using ^{129}Xe and ^{131}Xe is easily miniaturized, which has attracted considerable attention [2]. However, the relaxation time of ^{129}Xe and ^{131}Xe is much shorter than that of cryogenic ^3He . As a result, it is better to operate such an NMRG in a closed-loop mode, where a feedback driving field is applied [11]. Due to these differences, the previous analysis cannot be directly applied to miniature NMRGs. Miniature NMRGs have been mainly developed for use in strap-down inertial navigation systems, which not only need high precision but also a low cross-axis sensitivity [13]. Therefore, it is important to analyze the cross-axis coupling effects in an NMRG based on ^{129}Xe and ^{131}Xe .

In this paper, we established a theoretical model for the spin oscillator to analyze the cross-coupling effects in a $^{129}\text{Xe}/^{131}\text{Xe}$ NMRG. We find that these effects lead to a shift in the Larmor frequency, i.e., a measurement error in the NMRG. When the mechanical vibration contains a cross-axis rotation component near the Larmor frequency, the error will be very large. Moreover, this may result in the oscillation frequency being locked to the mechanical vibration rate, which destroys the NMRG's ability to measure the rotation rate. These results are of significance to the design of an NMRG and its corresponding strap-down inertial navigation system.

2. Theoretical Analysis

2.1. Principle of an NMRG

An NMRG using ^{129}Xe and ^{131}Xe is, in fact, a dual-species spin oscillator, as is shown in Figure 1 [1,11,14,15]. A vapor cell contains a mixture of gases, including $^{129}\text{Xe}/^{131}\text{Xe}$, N_2 and so on. To obtain angular momentum from the pump light, an excess amount of ^{87}Rb is filled into the vapor cell. When heated, the ^{87}Rb will vaporize and absorb pump light. The pump light is circularly polarized, so each photon carries angular momentum equal to one \hbar in the propagating direction. After taking in the circularly polarized photons, the spin of the ^{87}Rb atom will align along the z-direction, i.e., become polarized. Through spin-exchange collisions, the angular momentum transfers from the ^{87}Rb spins to the $^{129}\text{Xe}/^{131}\text{Xe}$ nuclear spins. As a result, the $^{129}\text{Xe}/^{131}\text{Xe}$ nuclear spins become polarized and give rise to a magnetization M . A linearly polarized probe light transmits through the cell and interacts with the polarized ^{87}Rb atoms. The polarization plane of the transmission light varies with the magnetic field sensed by the ^{87}Rb atoms. Therefore, the magnetization of the nuclear spins can be detected. The output of the detector is sent to a signal processing system, which is used to obtain the magnetic field in the x and y directions. The y-axis magnetization component M_y is amplified in the gain module, shifted by a phase of Φ , and then applied to drive the X-coil. For an appropriate gain and phase shift, the nuclear spins will precess continuously. More details for the NMRG can be found in [1].

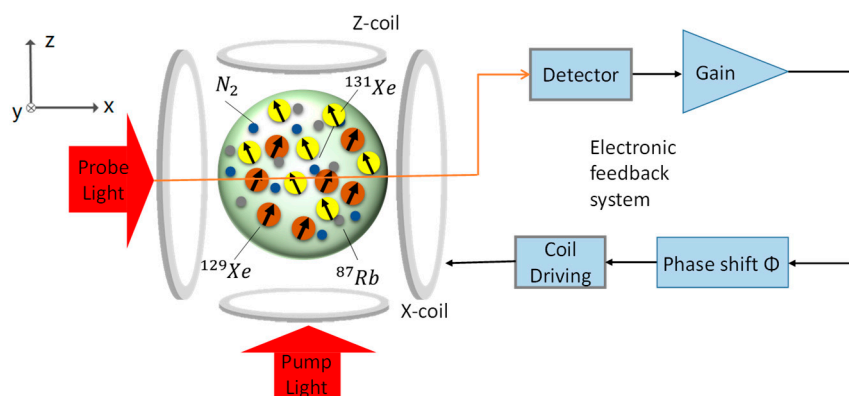


Figure 1. Principle of a dual-species spin oscillator.

The spin oscillator shown in Figure 1 actually has two spin oscillators: a ^{129}Xe oscillator and a ^{131}Xe oscillator. The ^{129}Xe and ^{131}Xe spins show negligible interaction through direct spin interaction, but coupling through the driving coil can occur. The driving fields of ^{129}Xe and ^{131}Xe influence each other, but this is not our concern here. In the following derivation, we will take the ^{129}Xe spin oscillator as an example to describe the operating principle.

The motion of the spins satisfies the following Bloch equation [10,12]:

$$\frac{d}{dt}\mathbf{M} = \mathbf{M} \times (\gamma\mathbf{B} + \mathbf{\Omega}), \quad (1)$$

where \mathbf{M} is the magnetization of the spins, γ is the gyromagnetic ratio, \mathbf{B} is the magnetic field and $\mathbf{\Omega}$ is the rotation rate of the gyroscope with respect to the inertial frame.

Equation (1) shows that the rotation has the same effect as a magnetic field $\mathbf{B}_{eff} = \mathbf{\Omega}/\gamma$. Thus, we will discuss cross-coupling effects using the following equation:

$$\frac{d}{dt}\mathbf{M} = \mathbf{M} \times \gamma\mathbf{B}. \quad (2)$$

Taking the relaxation time into account, Equation (2) can be expanded into the motion equation for the components of the magnetization:

$$\begin{cases} \frac{dM_x}{dt} = \gamma(M_y B_z - M_z B_y) - \frac{M_x}{T_2} \\ \frac{dM_y}{dt} = \gamma(M_z B_x - M_x B_z) - \frac{M_y}{T_2} \\ \frac{dM_z}{dt} = \gamma(M_x B_y - M_y B_x) + \frac{M_0 - M_z}{T_1} \end{cases}, \quad (3)$$

where M_x , M_y and M_z are the three components of the magnetization \mathbf{M} , respectively; B_x , B_y and B_z are the three components of the magnetic field, respectively; T_1 and T_2 are the longitudinal spin relaxation time and the transverse relaxation time, respectively.

Defining a complex vector $M_+ = M_x + iM_y$, and, from Equation (3), we can obtain:

$$\begin{cases} \frac{dM_+}{dt} = -i\gamma B_z M_+ + i\gamma M_z (B_x + iB_y) - \frac{M_+}{T_2} \\ \frac{dM_z}{dt} = \gamma(M_x B_y - M_y B_x) + \frac{M_0 - M_z}{T_1} \end{cases}. \quad (4)$$

To achieve analytical expressions for the oscillation frequency and amplitude for the ^{129}Xe spin oscillator, we posit the following hypothesis. A static magnetic field with magnitude $B_z = B_0$ is applied along the z -axis, and a field $B_x^d = 2D \cos(\omega_0 t)$ is applied along the x -axis to drive the spins. The feedback system has limited bandwidth so that the components with a frequency out of the range of $\omega \pm \Delta\omega_f$ are filtered out. Here, $\Delta\omega_f$ is the bandwidth of the filter. Through adjusting the phase shift and gain in the feedback loop, the spin magnetization precesses about the z -axis with frequency ω_0 in a clockwise manner. Therefore, we can write the following expressions:

$$\begin{aligned} M_x &= M_{x0} \cos(\omega_0 t) + M_{y0} \sin(\omega_0 t) \\ M_y &= -M_{x0} \sin(\omega_0 t) + M_{y0} \cos(\omega_0 t) \end{aligned} \quad (5)$$

where M_{x0} and M_{y0} are the components in the x and y -axes at $t = 0$, respectively.

With a rotating wave approximation, we can describe the driving magnetic field for ^{129}Xe as follows:

$$\begin{aligned} B_x^d &= D \cos(-\omega_0 t) \\ B_y^d &= D \sin(-\omega_0 t) \end{aligned} \quad (6)$$

Inserting Equations (5) and (6) into Equation (4), we have:

$$\begin{aligned} M_{+0} &= i\gamma DM_{z0}T_2 \\ \gamma DM_{y0} &= \frac{M_0 - M_{z0}}{T_1}, \end{aligned} \quad (7)$$

where $M_{+0} = M_{x0} + iM_{y0}$ and M_{z0} is the M_z in the steady state.

2.2. Modeling of a Spin Oscillator with a Cross-Axis-Rotation-Equivalent Magnetic Field

The influence of the cross-axis-rotation can be modeled by a transverse magnetic field; we might as well call this the cross-axis-rotation-equivalent (CARE) magnetic field. Without loss of generality, the CARE magnetic field can be described as follows:

$$\begin{aligned} B_x^e &= \sum_n B_n \cos(-\omega_n t - \varphi_n) \\ B_y^e &= \sum_n B_n \sin(-\omega_n t - \varphi_n) \end{aligned} \quad (8)$$

where B_n , ω_n and $-\varphi_n$ are the amplitude, angular frequency and phase of the n -th component, respectively.

With the CARE magnetic field, the motion of the spin oscillator still satisfies Equation (4), where $B_x = B_x^d + B_x^e$, $B_y = B_y^d + B_y^e$. We assume that the spins still precess around the z -axis but that the angular frequency of B_x^d and B_y^d changes from ω_0 to ω because of the CARE magnetic field; thus, we obtain the following expressions for the solutions of Equation (4):

$$\begin{aligned} M_{+} &= (M_{\perp 0} + M_{\perp}^*)e^{-i\omega t} = M_{\perp}e^{-i\omega t} \\ M_z &= M_{z0} + M_z^* \end{aligned} \quad (9)$$

where M_{\perp}^* and M_z^* are variations of the transverse and longitudinal magnetization due to the CARE magnetic field.

Inserting Equations (8) and (9) into Equation (4), we have:

$$\begin{aligned} \frac{dM_{+}}{dt} + i\gamma B_0 M_{+} + \frac{M_{+}}{T_2} &= i\gamma M_z \left(D e^{-i\omega t} + \sum_n B_n e^{-i\omega_n t - \varphi_n} \right) \\ \frac{dM_z}{dt} &= -\gamma DM_{y0} + \gamma M_{x0} \sum_n B_n \sin(\omega t - \omega_n t - \varphi_n) - \gamma M_{y0} \sum_n B_n \cos(\omega t - \omega_n t - \varphi_n) + \frac{M_0 - M_z}{T_1} \end{aligned} \quad (10)$$

Substituting Equations (7) and (9) into Equation (10), we have:

$$M_z^* \approx -\frac{1}{2}\gamma \sum_n B_n \left[\frac{M_{y0} + iM_{x0}}{1/T_1 + i(\omega - \omega_n)} e^{i(\omega - \omega_n)t - i\varphi_n} - \frac{iM_{x0} - M_{y0}}{1/T_1 - i(\omega - \omega_n)} e^{-i(\omega - \omega_n)t + i\varphi_n} \right], \quad (11)$$

and:

$$\frac{dM_{\perp}}{dt} + \frac{M_{\perp}}{T_2} - i(\omega - \omega_0)M_{\perp} = i\gamma [M_{z0} + M_z^*] \left(D + \sum_n B_n e^{i(\omega - \omega_n)t - i\varphi_n} \right). \quad (12)$$

Since the response of M_{\perp} to an alternating magnetic field with angular frequency larger than $1/T_2$ is small, we might as well neglect terms that contain $e^{i(\omega - \omega_n)t - i\varphi_n}$ in Equation (12). As a result, Equation (12) can be reduced to:

$$\frac{d}{dt}M_{\perp}^* + \frac{1}{T_2}M_{\perp}^* - i(\omega - \omega_0)(M_{\perp 0} + M_{\perp}^*) = -(M_{\perp 0} + M_{\perp}^*) \sum_n \frac{1}{2}(\gamma B_n)^2 \frac{1/T_1 + i(\omega - \omega_n)}{(1/T_1)^2 + (\omega - \omega_n)^2}, \quad (13)$$

Using the approximation that M_{\perp}^* varies very slowly with time, we obtain the following equation from Equation (13):

$$\omega = \omega_0 + \sum_n \frac{1}{2} (\gamma B_n)^2 \frac{(\omega - \omega_n)}{(1/T_1)^2 + (\omega - \omega_n)^2} \approx \omega_0 + \sum_n \frac{1}{2} (\gamma B_n)^2 \frac{(\omega_0 - \omega_n)}{(1/T_1)^2 + (\omega_0 - \omega_n)^2}. \quad (14)$$

In a practical case, the CARE field is usually small, so we replace the oscillating frequency ω with ω_0 in the last term of Equation (14) to avoid the difficulty in solving the oscillating frequency. The validity of the approximation can be proved in the following simulation.

Equation (14) gives the Bloch–Siegert shift formula for spin oscillators [16–18]. It is clear that when $\omega_0 > \omega_n$, $\Delta\omega = \omega - \omega_0 > 0$ and vice versa. Thus, the rotating field B_n pushes the oscillation frequency farther away from ω_n . When $\omega_n = -\omega_0$ and $B_n = D$, Equation (14) can be written as:

$$\omega = \omega_0 + \frac{(\gamma D)^2}{4\omega_0}. \quad (15)$$

This is just the case of a Bloch–Siegert shift for only one linear driving magnetic field. When $\omega_n = 0$ and $B_n = D$, Equation (14) can be written as:

$$\omega \approx \omega_0 + \frac{(\gamma D)^2}{2\omega_0}. \quad (16)$$

This is just the case of a cross-axis sensitivity effect when there is a static magnetic field in the xy-plane.

We can also obtain an approximate solution for M_{\perp} from Equation (13) for only one CARE component, $B_1 e^{-i\omega_1 t}$:

$$M_{\perp} = M_{\perp 0} + M_{\perp}^* \approx \frac{1/T_2}{1/T_2 + \frac{1}{2}\omega_1^2 \frac{1/T_1}{(1/T_1)^2 + (\omega - \omega_1)^2}} M_{\perp 0}. \quad (17)$$

where $\omega_1 = \gamma B_1$.

When $\omega_n \rightarrow \omega_0$, Equation (17) becomes:

$$M_{\perp} = \frac{1}{1 + \frac{1}{2}\omega_1^2 T_1 T_2} M_{\perp 0}. \quad (18)$$

This means that if the CARE magnetic field has the same frequency as ω_0 , the amplitude of the spin oscillator decreases. However, when $|\omega_n - \omega_0|$ is less than a specific value, the spin oscillator will be locked to the CARE field [19]. As a result, Equation (18) will not be valid. This can be seen in the following derivation. We assume there is only one component with frequency ω_r near ω_0 , so we neglect other components. The CARE magnetic field can be described as:

$$B_x^e = B_r \cos(-\omega_r t), B_y^e = B_r \sin(-\omega_r t), \quad (19)$$

and the feedback magnetic field can be described as:

$$B_x^d = D \cos(-\omega_r t - \psi), B_y^d = D \sin(-\omega_r t - \psi). \quad (20)$$

where ψ is a time varying phase.

We use the following expressions for the solutions of the Bloch equation:

$$\begin{aligned} M_+ &= (M_{\perp 0} + M_{\perp}^*) e^{-i(\omega_r t + \psi)} = M_{\perp} e^{-i(\omega_r t + \psi)} \\ M_z &= M_{z0} + M_z^* \end{aligned} \quad (21)$$

Inserting Equations (19)–(21) into Equation (4), we have:

$$\begin{aligned} \frac{dM_+}{dt} + i\gamma B_0 M_+ + \frac{M_+}{T_2} &= i\gamma M_z (De^{-i(\omega_r t + \psi)} + B_r e^{-i\omega_r t}) \\ \frac{dM_z}{dt} &= -\gamma D(M_{y0} + M_y^*) + \gamma B_r [(M_{x0} + M_x^*) \sin \psi - (M_{y0} + M_y^*) \cos \psi] + \frac{M_0 - M_z}{T_1} \end{aligned} \quad (22)$$

Substituting Equation (7) into Equation (22), we have:

$$\frac{dM_z^*}{dt} + \frac{M_z^*}{T_1} = -\gamma D M_y^* + \gamma B_r [(M_{x0} + M_x^*) \sin \psi - (M_{y0} + M_y^*) \cos \psi], \quad (23)$$

and:

$$-i\left(\omega_r - \omega_0 + \frac{d\psi}{dt}\right)(M_{+0} + M_+^*) + \frac{1}{T_2} M_+^* = i\gamma M_z^* (D + B_r e^{i\psi}) + i\gamma M_{z0} B_r e^{i\psi}. \quad (24)$$

We make the approximation that $d^2\psi/dt^2 = 0$ and obtain M_z^* from Equation (23):

$$M_z^* = -\gamma D M_y^* + \frac{\gamma B_r}{2\left(\frac{1}{T_1} + i\frac{d\psi}{dt}\right)} [-iM_x^* - (M_{y0} + M_y^*)] e^{i\psi} + \frac{\gamma B_r}{2\left(\frac{1}{T_1} - i\frac{d\psi}{dt}\right)} [iM_x^* - (M_{y0} + M_y^*)] e^{-i\psi}, \quad (25)$$

Using the approximation that M_{\perp}^* varies slowly with time, we obtain the following equation:

$$\begin{aligned} -i\left(\omega_r - \omega_0 + \frac{d\psi}{dt}\right)(M_{+0} + M_+^*) + \frac{1}{T_2} M_+^* &= -i(\gamma D)^2 M_y^* + i\gamma B_r M_{z0} e^{i\psi} - i\gamma^2 D B_r M_y^* e^{i\psi} \\ &+ i\frac{\gamma^2 D B_r}{2} \left(\frac{[-iM_x^* - (M_{y0} + M_y^*)]}{(1/T_1 + i\frac{d\psi}{dt})} e^{2i\psi} + \frac{[iM_x^* - (M_{y0} + M_y^*)]}{(1/T_1 - i\frac{d\psi}{dt})} \right) \\ &+ i\frac{(\gamma B_r)^2}{2} \left(\frac{[-iM_x^* - (M_{y0} + M_y^*)]}{(1/T_1 + i\frac{d\psi}{dt})} e^{2i\psi} + \frac{[iM_x^* - (M_{y0} + M_y^*)]}{(1/T_1 - i\frac{d\psi}{dt})} \right) \end{aligned} \quad (26)$$

Neglecting the terms containing $e^{2i\psi}$, Equation (26) can be reduced to:

$$\begin{aligned} -i\left(\omega_r - \omega_0 + \frac{d\psi}{dt}\right)(M_{+0} + M_+^*) + \frac{1}{T_2} M_+^* &= -i(\gamma D)^2 M_y^* + i\gamma B_r M_{z0} e^{i\psi} - i\gamma^2 D B_r M_y^* e^{i\psi} \\ &+ i\frac{\gamma^2 D B_r}{2} \left(\frac{[iM_x^* - (M_{y0} + M_y^*)]}{(1/T_1 - i\frac{d\psi}{dt})} \right) + i\frac{(\gamma B_r)^2}{2} \left(\frac{[iM_x^* - (M_{y0} + M_y^*)]}{(1/T_1 - i\frac{d\psi}{dt})} \right) \end{aligned} \quad (27)$$

This equation can be expressed as:

$$\frac{d\psi}{dt} = \omega_0 - \omega_r + d + l \cos(\psi - \psi_0). \quad (28)$$

where d , l and ψ_0 are functions of M_{+0} , M_{\perp}^* , B_r , T_2 and T_1 . Equation (28) indicates that the spin oscillator can be locked to the CARE magnetic field when $|\omega_0 - \omega_r + d| < |l|$. This phenomenon is similar to the lock-in in ring laser gyroscopes [20,21]. A comprehensive analysis can be seen in [19].

We can obtain the lock-in threshold l from Equation (27):

$$l \approx \gamma B_r M_{z0} / M_{+0}. \quad (29)$$

The expression of l is consistent with the lock-in threshold with the rotating CARE case given in [19], since we have made rotating wave approximation in this paper. According to [11], the maximum of M_{+0} is $M_0 \sqrt{T_2} / (2 \sqrt{T_1})$ and the corresponding M_{z0} is $M_0 / 2$. Under this condition, we have:

$$l \approx \gamma B_r \sqrt{T_1 / T_2}. \quad (30)$$

3. Numerical Simulation and Discussion

We carry out numerical simulation according to Equation (3). The simulation model based on Figure 1 is shown in Figure 2. The feedback magnetic field is $B_x^d = kM_y$, $B_y^d = kM_x$ and the CARE magnetic field is $B_x^e = B_r \cos(-\omega_r t)$, $B_y^e = B_r \sin(-\omega_r t)$. The parameters are as follows: $T_1 = 30$ s, $T_2 = 20$ s, $B_0 = 1.5$ μ T, $\gamma = 2\pi \times 10$ Hz/ μ T, $M_{z0} = 100$ A/m, $k = 0.0015$. The initial values for the magnetization components are $M_x = 0.01M_{z0}$, $M_y = 0$ and $M_z = M_{z0}$, respectively. Other parameters will be given in the specific simulation.

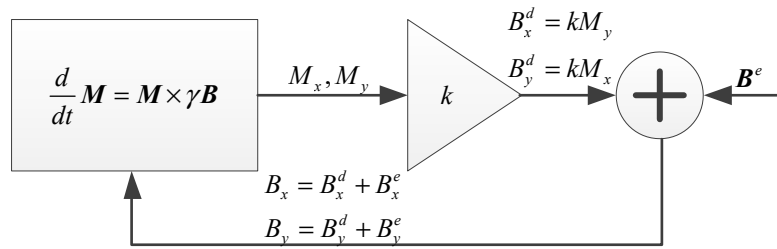


Figure 2. Simulation model corresponding to the NMRG principle given in Figure 1.

The Bloch equations were solved using the MATLAB ODE45 solver. The time step was 50 μ s, and the time span was 0–1000 s. When we obtain the magnetization $M(t)$, we use the $M_y(t)$ with a time span of 400 s–1000 s to make a fast Fourier transformation (FFT). We obtain the amplitude and frequency of the spin oscillator according to the peak in the FFT. With a timespan of 600 s, the frequency resolution is 0.0017 Hz and the obtained amplitude also shows errors due to limited data.

3.1. Frequency Shift due to a DC Magnetic Field

In this case, the CARE magnetic field is $B_x^e = 0$, $B_y^e = B_r$. In theory, the approximate analytical expression for the oscillation frequency shift will be $\Delta f = \frac{\omega - \omega_0}{2\pi} = \frac{1}{2\pi} \frac{(\gamma B_r)^2}{2\omega_0}$. The simulation and approximate results are shown in Figure 3. It is clear that the approximate analytical results agree well with the numerical simulation results.

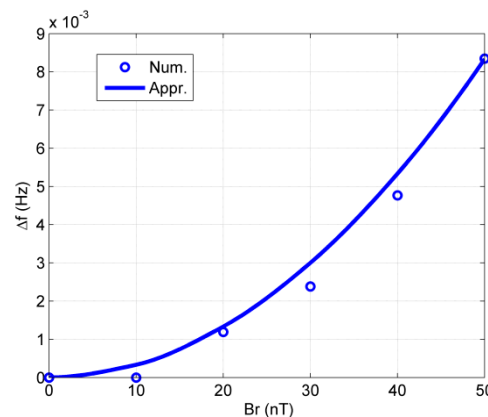


Figure 3. The frequency shift vs. DC magnetic field in the y -axis. “Num.” and “Appr.” in the figure denote numerical and approximate analytical results, respectively.

According to $B_y^{eq} = \Omega_y / \gamma$ we know that the rotation for the y -axis will lead to an equivalent magnetic field. When the NMRG is placed in a vehicle, the maximum value of Ω_y can be as high as 2π rad/s, equivalent to a magnetic field of 78 nT for the ^{129}Xe spin oscillator and 284 nT for the ^{131}Xe spin oscillator. When $B_0 = 12$ μ T, the frequency shifts for ^{129}Xe and ^{131}Xe are 3.5 mHz and 11.8 mHz, respectively. This is a huge error for the NMRG, since it should measure Ω_z with an error of less than 10 nHz for typical applications. To suppress this cross-axis effect, some methods can be

used. For example, with a three-dimensional magnetic field compensation [22], the influence of low frequency Ω_y can be suppressed greatly, but the bandwidth of the feedback loop should be as high as possible.

3.2. Frequency Shift due to an Oscillating Magnetic Field

3.2.1. One Component

At first, we carry out simulations for the CARE magnetic field with only one frequency, where $B_x^e = B_r \cos(-\omega_r t)$, $B_y^e = B_r \sin(-\omega_r t)$. According to a previous analysis, the approximate frequency shift will be $\Delta f = \frac{1}{4\pi} \gamma^2 B_r^2 \frac{1}{\omega_0 - \omega_r}$. We choose two ω_r values and make the Δf curve a function of B_r . The simulation and approximate results are shown in Figure 4. The approximate analytical results agree well with the numerical simulation results.

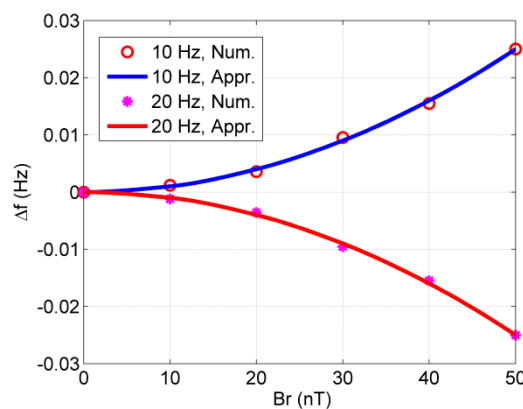


Figure 4. The frequency shift vs. B_r for different frequencies of the Cross-Axis-Rotation-Equivalent (CARE) magnetic field.

Next, at a specific magnetic field B_r , we change the frequency f_r . The frequency shift $\Delta f = \frac{1}{4\pi} \frac{\gamma^2 B_r^2}{\omega_0 - \omega_r}$ and amplitude $Amp = \frac{1/T_2}{1/T_2 + \frac{1}{2} \gamma^2 B_r^2 \frac{1/T_1}{(1/T_1)^2 + (\omega - \omega_n)^2}} Amp_0$ of the spin oscillator are given in Figure 5. Here,

Amp_0 denotes the amplitude of the spin oscillator without a CARE field. When $\omega_r \rightarrow \omega_0$, $|\Delta f|$ becomes very large. The relaxation time T_1 removes the frequency shift singular point when $\omega_r \rightarrow \omega_0$. At a specific B_r , the spin oscillator is locked to the CARE magnetic field and its frequency is equal to ω_r . We also find that when ω_r approaches ω_0 , the approximation solution has a larger error. The reason for this is that when ω_r approaches ω_0 , we omitted some terms containing $e^{i(\omega - \omega_n)t}$ in the derivation for Equations (11) and (13). The approximation for Amp has a slightly larger error, but it still agrees with the numerical simulation qualitatively. That is, the CARE magnetic field near the Larmor frequency reduces the amplitude of the spin oscillator. It should be noted that the simulation program from Equation (3) also contributes to some error, which leads to the numerical data dispersion shown in Figure 5c,d.

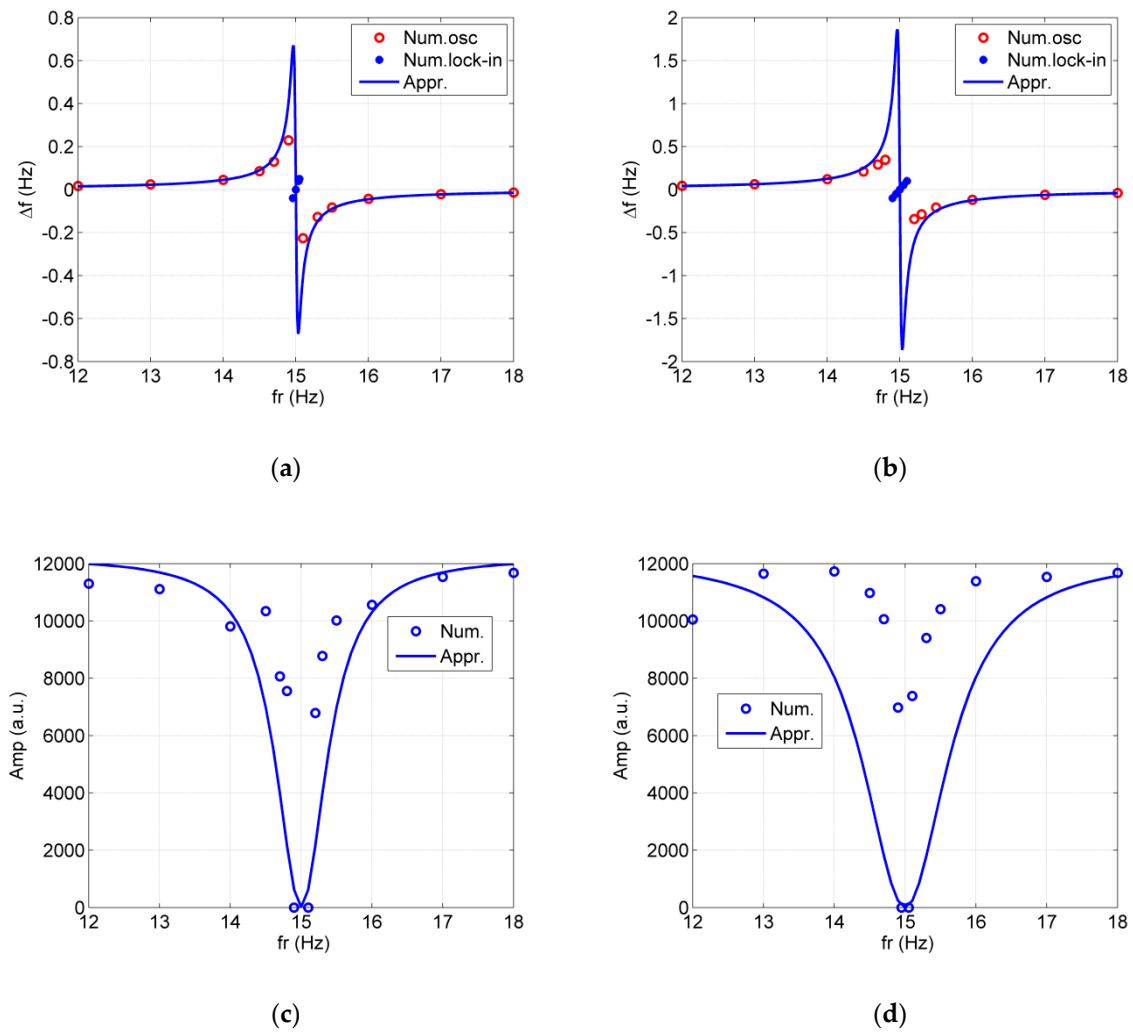


Figure 5. The frequency shift Δf and amplitude Amp of the spin oscillator vs. frequencies of the CARE magnetic field. (a) Δf vs. f_r for $B_r = 30$ nT; (b) Δf vs. f_r for $B_r = 50$ nT; (c) Amp vs. f_r for $B_r = 30$ nT; (d) Amp vs. f_r for $B_r = 50$ nT. In (a,b), Num. lock-in denotes the frequency shift in the lock-in state. In the lock-in state of (c,d), we let Amp = 0 to express that the spin oscillator cannot normally measure the rotation rates. In fact, the amplitude and frequency of the spin oscillator in the lock-in state is governed by the CARE magnetic field. The limited data for FFT contribute to the scattering of frequency shift and Amp to some extent.

3.2.2. Two Harmonic Components

To check the approximate frequency shift in Equation (14) when the CARE magnetic field has more frequency components, we choose $B_x^e = B_{r1} \cos(-\omega_{r1}t) + B_{r2} \cos(-\omega_{r2}t)$ and $B_y^e = B_{r1} \sin(-\omega_{r1}t) + B_{r2} \sin(-\omega_{r2}t)$ to carry out numerical simulations. The approximate frequency shift is $\Delta f = \frac{1}{4\pi} \gamma^2 B_r^2 \left(\frac{1}{\omega_0 - \omega_{r1}} + \frac{1}{\omega_0 - \omega_{r2}} \right)$. Here, we choose $B_{r1} = B_{r2} = B_r$. The results are shown in Figure 6, which shows that the approximate frequency shift agrees well with the numerical simulation.

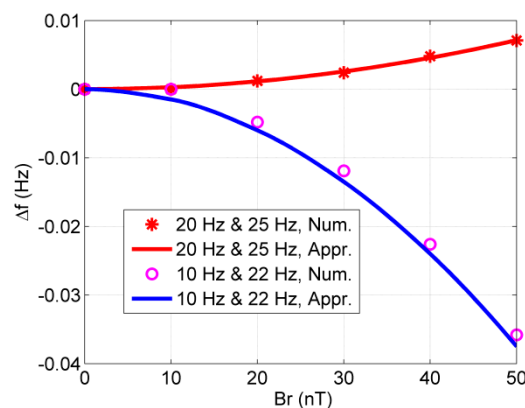


Figure 6. The frequency shift vs. magnetic field amplitude for different groups of magnetic fields. Two groups of magnetic field are given: one is $f_{r1} = 20$ Hz and $f_{r2} = 25$ Hz while another is 10 Hz and $f_{r2} = 22$ Hz.

3.3. Discussions

3.3.1. Comparing the ^3He Gyroscope with a Dual-isotope Xe NMRG

Both the amplitude and frequency of the spin oscillator are changed due to the CARE magnetic field. The dynamical equation for analyzing the ^3He gyroscope omitted the relaxation times T_1 and T_2 in Equation (3) and did not need the driving magnetic field. Therefore, the two types of gyroscopes are expected to show different behavior.

For a CARE magnetic field with very low frequency, the frequency shift for the two gyroscopes can be described by Equation (16). However, when the frequency of the CARE magnetic field is near the Larmor frequency, the ^3He gyroscope loses signal periodically, and the amplitude of the Xe NMRG signal decreases. For the oscillation frequency of the Xe spin oscillator, it is locked to the frequency of the CARE magnetic field, and, out of the lock-in range, the oscillation frequency shifts according to Equation (14). This shows the CARE magnetic field pushes the oscillation frequency of a spin oscillator far away from the CARE magnetic field frequency. Therefore, the CARE magnetic field cannot be common-mode suppressed effectively by a dual-isotope scheme.

3.3.2. Methods to Reduce the Cross-Axis Effect

If the CARE magnetic field results from the rotation of a vehicle, it has a low frequency. Therefore, it is clear that we can reduce the cross-axis effect by increasing B_0 . Assuming a cross-axis input rotation rate of 1 rad/s, B_0 should be larger than 0.049 T for a ^3He gyroscope [10]. This is not practical, since the magnetic inhomogeneity can be very large at this magnetic field. Fortunately, the transverse magnetic field in Xe NMRGs can be compensated by an alkali atom magnetometer and a feedback loop [22]. In general, a compensation bandwidth of approximately 10 Hz can be obtained.

For a high-frequency CARE magnetic field, the compensation loop cannot follow it in a timely manner. If the frequency spectrum of the angular vibration covers the Larmor frequency of the spin oscillator, it will cause a severe error. We might as well take the rotation component around the y -axis as an example to discuss the influence of the angular vibration [23,24]. We assume the rotation component has an amplitude of 0.003 rad/s at 100 Hz, corresponding to $B_y^{eq} = 0.04$ nT for ^{129}Xe and $B_y^{eq} = 0.13$ nT for ^{131}Xe . When $B_0 = 10$ μT , the frequency shifts of ^{129}Xe and ^{131}Xe due to the CARE magnetic field are 12.8 μHz and -3.7 μHz , respectively. Moreover, the worst case is a lock-in phenomenon, which makes the NMRG unresponsive toward Ω_z . With $T_1 = T_2 = 25$ s, $\gamma B_r = 0.003$ rad/s and the lock-in threshold is approximately 0.17 $^\circ/\text{s}$. It is a severe error for an NMRG.

To improve the tolerance of the NMRG toward the cross-axis angular vibration, it is better to choose a stronger B_0 , to ensure that the Larmor frequency is far away from the angular vibration

component. The system level vibration isolation can also be used to attenuate possible angular vibration. In order to solve the lock-in problem, we can also use the biasing method just as that in ring laser gyroscopes, but it will make the NMRG more complicated.

4. Conclusions

In summary, we analyzed the response of a spin oscillator to a magnetic field in the xy -plane with both analytical and numerical methods. Approximate analytical equations for the frequency shift and amplitude of the spin oscillator with the CARE field are obtained, which are verified by solving the Bloch equations numerically. Then, we discussed the measurement error in an NMRG due to a rotation component in the x or y -axis. The NMRG is a single-axis gyroscope, but it also has cross-axis sensitivity to the x and y -axis. If the NMRG is subject to cross-axis rotation with a frequency near to its magnetic resonance frequency, the measurement error is relatively large, and the rotation rate cannot be measured. To reduce the cross-axis coupling effect, the resonance magnetic field should be as large as possible and a mechanical notch filter covering the oscillating frequencies of ^{129}Xe and ^{131}Xe can be used. These problems should be considered in the design of NMRG-based strap-down inertial navigation systems.

Author Contributions: Conceptualization, Z.W. and H.L.; methodology, Z.W.; software, Z.W.; validation, Y.Z., X.Z. and Q.J.; writing—original draft preparation, Z.W.; writing—review and editing, Z.W., Y.Z., X.Z. and Q.J.; project administration, Z.W. and H.L.; funding acquisition, Z.W. and H.L. All authors have read and agreed to the published version of the manuscript.

Funding: This research was funded by the National Natural Science Foundation of China (Grant No. 61671458, 61701515), the Natural Science Foundation of Hunan (Grant No. 2018JJ3608) and the Research Project of the National University of Defense Technology (Grant No. ZK170204), China Postdoctoral Science Foundation (Grant No. 2017M613367).

Conflicts of Interest: The authors declare no conflicts of interest.

References

1. Eklund, E.J. Microgyroscope Based on Spin-Polarized Nuclei. Ph.D. Thesis, University of California, Irvine, CA, USA, 2008.
2. Walker, T.G.; Larsen, M.S. Spin-Exchange Pumped NMR Gyros. *Adv. Atom. Mol. Opt. Phys.* **2016**, *65*, 373–401.
3. Larsen, M.; Bulatowicz, M. Nuclear magnetic resonance gyroscope. *IEEE Freq. Control Symp.* **2012**, 978, 1–5.
4. Donley, E. Nuclear magnetic resonance gyroscopes. In Proceedings of the SENSORS, 2010 IEEE, Kona, HI, USA, 1–4 November 2010.
5. Meyer, D.; Larsen, M. Nuclear magnetic resonance gyro for inertial navigation. *Gyroscopy Navig.* **2014**, *5*, 75–82. [[CrossRef](#)]
6. Woodman, K.F.; Franks, P.W.; Richards, M.D. The nuclear magnetic resonance gyroscope: A review. *J. Navig.* **1987**, *40*, 366–384. [[CrossRef](#)]
7. Fang, J.C.; Qin, J. Advances in atomic gyroscopes: A view from inertial navigation applications. *Sensors* **2012**, *12*, 6331–6346. [[CrossRef](#)] [[PubMed](#)]
8. Qin, J.; Wang, S.; Gao, P.; Wang, Y.; Han, W. Advances in nuclear magnetic resonance gyroscope. *Navig. Positioning Timing* **2014**, *1*, 64–69.
9. Shaw, G.L. Sensitivity to cross-axis oscillations in a single-axis nuclear gyroscope. *J. Guid. Control Dynam.* **1984**, *7*, 501–502. [[CrossRef](#)]
10. Shaw, G.L. ^3He Nuclear Gyroscope. Available online: <https://apps.dtic.mil/dtic/tr/fulltext/u2/a159924.pdf> (accessed on 29 January 2020).
11. Wang, Z.G.; Peng, X.; Luo, H.; Guo, H. Comparison of operation modes for spin-exchange optically-pumped spin oscillators. *J. Magn. Reson.* **2017**, *278*, 134–140. [[CrossRef](#)] [[PubMed](#)]
12. Abragam, A. *The Principles of Nuclear Magnetism*; Oxford University Press: London, UK, 1961.
13. Guerinoni, L.; Falorni, G.L.; Gattere, G. Modelling Cross Axis Sensitivity in MEMS Coriolis Vibratory Gyroscopes. *Proceedings* **2017**, *1*, 281. [[CrossRef](#)]

14. Bulatowicz, M.; Griffith, R.; Larsen, M.; Mirjaniyan, J.; Fu, C.B.; Smith, E.; Snow, W.M.; Yan, H.; Walker, T.G. Laboratory search for a long-range T-Odd, P-Odd interaction from axionlike particles using dual-species nuclear magnetic resonance with polarized ^{129}Xe and ^{131}Xe gas. *Phys. Rev. Lett.* **2013**, *111*, 102001. [[CrossRef](#)] [[PubMed](#)]
15. Yoshimi, A.; Asahi, K.; Sakai, K.; Tsuda, M.; Yogo, K.; Ogawa, H.; Suzuki, T.; Nagakura, M. Nuclear spin maser with an artificial feedback mechanism. *Phys. Lett. A* **2002**, *304*, 13–20. [[CrossRef](#)]
16. Pendlebury, J.M.; Heil, W.; Sobolev, Y.; Harris, P.G.; Richardson, J.D.; Baskin, R.J.; Doyle, D.D.; Geltenbort, P.; Green, K.; van der Grinten, M.G.D.; et al. Geometric-phase-induced false electric dipole moment signals for particles in traps. *Phys. Rev. A* **2008**, *70*, 32102. [[CrossRef](#)]
17. Bloch, F.; Siegert, A. Magnetic resonance for nonrotating fields. *Phys. Rev.* **1940**, *57*, 522–527. [[CrossRef](#)]
18. Ramsey, N.F. Resonance transitions induced by perturbations at two or more different frequencies. *Phys. Rev.* **1955**, *100*, 1191–1194.
19. Pavlov, Y.V.; Pivkin, A.N.; Umarmkhodzhaev, R.M.; Lariontsev, E.G. Synchronization with harmonics in an injected nuclear-magnetic-resonance laser. *Phys. Rev. A* **2010**, *82*, 33802. [[CrossRef](#)]
20. Chow, W.W.; Gea-Banacloche, J.; Pedrotti, L.M.; Sanders, V.E.; Schleich, W.; Scully, M.O. The ring laser gyro. *Rev. Mod. Phys.* **1985**, *57*, 61–103. [[CrossRef](#)]
21. Krobka, N.I.; Türkin, D.A. Laser gyros frequency biasing and fiber optic gyros phase biasing: Similarities and differences. In Proceedings of the 2017 24th Saint Petersburg International Conference on Integrated Navigation Systems (ICINS), St. Petersburg, Russia, 29–31 May 2017.
22. Grover, B.C.; Kanegsberg, E.; Mark, J.G.; Meyer, R.L. Nuclear Magnetic Resonance Gyro. U.S. Patent 4,157,495, 5 June 1979.
23. Lee, J.P.; Whaley, W. Prediction of the angular vibration of aircraft structures. *J. Sound Vib.* **1976**, *49*, 541–549. [[CrossRef](#)]
24. Merritt, P.; Donaldson, J.; O'Brien, D.; Coleman, K.; Pyles, G. Angular vibration survey of various aircraft. In Proceedings of the Laser Systems Technology, Orlando, FL, USA, 21–25 April 2003.



© 2020 by the authors. Licensee MDPI, Basel, Switzerland. This article is an open access article distributed under the terms and conditions of the Creative Commons Attribution (CC BY) license (<http://creativecommons.org/licenses/by/4.0/>).